EUROFUSION WPMST1-PR(16) 15267

V Bobkov et al.

Making ICRF power compatible with high-Z wall in ASDEX Upgrade

Preprint of Paper to be submitted for publication in 43rd European Physical Society Conference on Plasma Physics (EPS)

This work has been carried out within the framework of the EUROfusion Consortium and has received funding from the Euratom research and training programme 2014-2018 under grant agreement No 633053. The views and opinions expressed herein do not necessarily reflect those of the European Commission.

Making ICRF power compatible with a high-Z wall in ASDEX Upgrade

V. Bobkov[1], D. Aguiam[2], R. Bilato[1], S. Brezinsek[3], L. Colas[4], H. Faugel[1], H. Fünfgelder[1], A. Herrmann[1], J. Jacquot[1], A. Kallenbach[1], D. Milanesio[5], R. Maggiora[5], R. Neu[1,6], J.-M. Noterdaeme[1,7], R. Ochoukov[1], S. Potzel[1], Th. Pütterich[1], A. Silva[2], W. Tierens[1], A. Tuccillo[8], O. Tudisco[8], Y. Wang[9], Q Yang[9], W. Zhang[1], ASDEX Upgrade Team and the EUROfusion MST1 Team

[1] *Max-Planck-Institut für Plasmaphysik, Boltzmannstr. 2, 85748 Garching, Germany*
[2] *Instituto de Plasmas e Fusão Nuclear, Instituto Superior Técnico, Universidade de Lisboa, 1049-001 Lisboa, Portugal*
[3] *Forschungszentrum Jülich GmbH, Institut für Energie- und Klimaforschung – Plasmaphysik, Partner of the Trilateral Euregio Cluster (TEC), 52425 Jülich, Germany*
[4] *IRFM, Association EUROFUSION -CEA, Saint-Paul-Lez-Durance, France*
[5] *Politecnico di Torino, Italy*
[6] *Technische Universität München, Boltzmannstr. 15, 85748 Garching, Germany*
[7] *Applied Physics Department, University of Ghent, Ghent, Belgium*
[8] *ENEA, Frascati, Italy*
[9] *ASIPP, Institute of Plasma Physics, Chinese Academy of Sciences, Hefei, China*

Abstract. Comparison of the ASDEX Upgrade 3-strap ICRF antenna data with the linear electromagnetic TOPICA calculations substantiates a reduction of the local electric field at the antenna radially protruding plasma facing elements as a relevant criterion for the minimization of the tungsten (W) sputtering in the conditions when the slow wave is strongly evanescent. Temporal and spatial fluctuations of the 3-dimensional plasma density distribution affected by local non-linear interactions are thought to be responsible for a less sensitive reaction of the time-averaged RF current at the antenna limiters to antenna feeding variations than predicted by the calculations. The 3-strap antenna with the W-coated limiters produces drastically less W sputtering compared to the W-coated 2-strap antennas. This is consistent with the non-linear asymptotic SSWICH calculations for RF sheaths.

Introduction

Operation of Ion Cyclotron Range of Frequencies (ICRF) antennas is often accompanied by parasitic processes such as impurity production and additional heat loads on plasma facing components (PFCs). These are thought to be to a significant part a consequence of the RF electrical fields near antenna, in particular the parallel field $E_{||}$. The latter is responsible for formation of RF sheaths by driving more mobile electrons to the antenna PFCs and charging up the plasma, as the PFCs are usually grounded. The RF sheaths are characterized by an elevated time-averaged or a DC potential drop close to conductive surfaces. This leads to the enhanced physical sputtering by accelerated ions and to the increased heat loads.

In all-tungsten ASDEX Upgrade (AUG), the ICRF specific W production had a strong influence on ICRF applicability due to increased radiation [1]. Whereas some aid to reduce the W production was found in tailoring the plasma properties in the scrape-off layer (SOL) by shifting the plasma radially away from the antenna [2] and by local gas injection [3], the installation of the boron (B)-coated limiters at the 2-strap antennas was the step to enlarge the ICRF operational window in AUG significantly. Although the root cause for the enhanced sputtering has not been removed by the use of the B-limiters, the ICRF operational window was enlarged significantly due to the fact that increase of content of the low-radiating low-Z boron is tolerable. In parallel, the antenna optimization was studied. As a first step, one of the 2-strap antennas was modified with broad-limiters and optimized straps which showed up to 40% reduction in W release [3]. A second, more advanced step was the installation of the new 3-strap antennas [3] in 2015 which constitutes the main subject of this paper.

This paper discusses the criteria for minimization of the RF sheath effects by optimization of the near-field distribution, considering the slow wave propagation in the

private antenna region in section 1 and a simplified approach used for the 3-strap antenna. Section 2 is devoted to the description of measurements, comparison to calculations and relations to the W sputtering. At the end the section summarizes the total effect of the 3-strap antennas on reduction of the W release.

1. Minimization of RF sheaths effects

1.1 Relevance of criteria for minimization of the effect of RF sheaths

The approach to calculate the integral of $E_{||}$ along a magnetic field line as an estimate of the sheath-driving RF voltage [4], $V_{RF\,sheath} = \left|\int E_{||}(\vec{l}) \cdot d\vec{l}\right|$ in the absence of the sheaths at the plasma-wall boundaries, was usually used in the past (see e.g. [5]) in order to characterize the effect of the RF near fields on the antenna-plasma interactions. This basic linear approach was simple to use, but its use is questionable from many points of view. Firstly, in contrast to [5], in many cases only the long field lines were considered which pass in front of an antenna [6, 7] without intersecting any conducting structure and are spatially limited just by the calculation frame. As a result, the calculated RF voltages, supposedly relevant for a local RF sheath formation deep in the private plasma region of an antenna, could strongly be influenced by the RF field excited in the remote locations not connected to this private region along the magnetic field lines. Secondly, the direct integration of $E_{||}$ implies perfect parallel plasma conductivity, not describing the fact that on RF timescale the conducting properties of the plasma are typically dominated by the plasma polarization effects and the displacement currents. Experimental application of this criteria resulted in the absence of a positive effect after the Tore Supra Faraday Screen (FS) was modified [8] and in an inconsistency between the calculations and the experimental observations in monopole phasing at Alcator C-Mod [9]. At the same time, the field-aligned antenna in Alcator C-Mod showed a significant reduction of impurity sources during ICRF with local ICRF impurity sources effectively eliminated. Recent experimental observations of heat flux to antenna components in Tore Supra [8] and of RF image currents on the frame of the imbalanced 2-strap antenna in ASDEX Upgrade [10] show that quantities relevant for the antenna-plasma interactions cannot be described by a single value for a given magnetic field line, because strong asymmetries are observed on opposite ends of the field line.

For the AUG antenna improvement, a different criterion was advocated in [2,3,11]. The reduction of the local $E_{||}$-field values close to the radially protruding antenna side limiters, i.e. conducting structures, was targeted. Here magnetic field lines intersect the conducting surfaces and high $E_{||}$-field can be excited if local RF currents exist. Presence of radially protruding structures also increases the electron losses with the resulting formation of RF sheaths. Far away from these structures along the magnetic field lines, electrons can show the oscillatory behaviour imposed by RF cycle. However the influence of the remote RF field excitation due to wave propagation was not taken into account in this approach. The recent work with the SSWICH code [12, 13] and an analytic formulation of the slow wave propagation and sheath boundary conditions [14] allow for further substantiation of the AUG approach. In [14], the weighted integration of $E_{||}$ along the field lines $V_{RF\,sheath}(\vec{r}) = \int G(\vec{r},\vec{r}_0) E_{||}(\vec{r}_0) \cdot d\vec{r}_0$ is proposed, in order to take into account the propagation of the slow wave in the presence of the sheaths at the plasma-wall boundaries. The slow wave is assumed to be the dominant contributor to $E_{||}$. Here, $G(\vec{r},\vec{r}_0)$ is the weighting function which depends on the position of the sheath boundary $\vec{r}$ (in AUG case – the limiters) for which the sheath oscillating voltage $V_{RF\,sheath}$ is calculated and on the position $\vec{r}_0$ of every $E_{||}$ wave emitting point on the aperture of the antenna (typically a toroidal-poloidal plane just in front of the antenna). Function $G(\vec{r},\vec{r}_0)$ describes how the slow wave transmits the $E_{||}$-field from its source to a point at the limiters where an RF sheath is formed. If this transmission is weak on a characteristic length of an antenna, the RF sheath is influenced by local $E_{||}$ only.

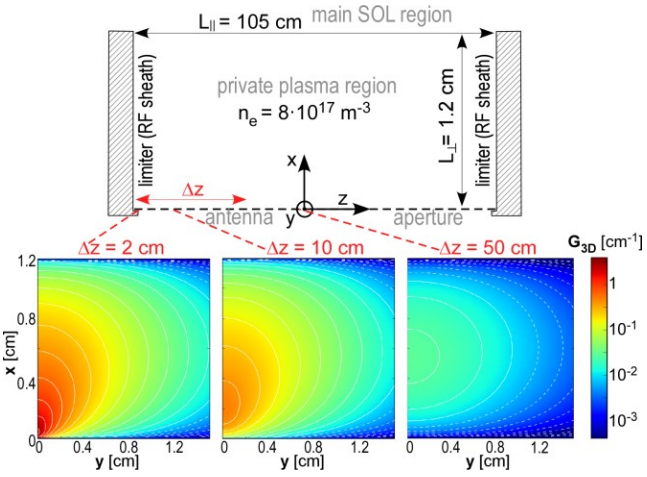

Figure 1. Geometry of calculations and weighting factor G_{3D} versus transverse coordinates (x,y), as evaluated numerically using parallel distances Δz=2 cm, Δz=10 cm, Δz=50 cm.

We estimate the slow wave transmission of $E_{||}$-field by calculating $G(\vec{r},\vec{r}_0)$ for the relevant AUG parameters: parallel length of $L_{||}$ = 1.05 m, perpendicular radial length (along x) of the protruding limiters $L_\perp$=0.012 m, plasma density in antenna private region n_e=8·10^{17} m^{-3} and RF frequency of 36.5 MHz. Figure 1 describes the geometry of the calculations and the 3D weighting function G_{3D} which is a 3D Green's function calculated according to [14]. Dimensions along y (mostly poloidal) in the calculation frame are assumed infinite. Values of G_{3D} imply integration along y separately from integration along a field line (z). A single point RF emitter is defined at Δz=0, x=0. The main feature of the figure is the strong parallel decay of the weighting factor. This is explained by the evanescent propagation of the slow wave at the frequency well above the lower hybrid frequency in the frame limited by the sheath boundary conditions which strongly influence the propagation. Function G_{3D} experiences a more than a factor of 10 decrease on a parallel distance of Δz=0.5 m which corresponds to about a half of toroidal dimension of the 3-strap antenna. The transverse poloidal distribution of the weighting function is about 1 cm broad and becomes more homogenous when parallel distance is increased. This is explained by a coupling of the slow wave field between neighbouring magnetic field lines.

Thus for the relevant AUG parameters, due to the strong parallel decay of the slow wave field it indeed can be reasonable to assume that the effect of the local $E_{||}$-field close to the locations where the RF sheaths are formed is dominant. At the same time the independent influence of the remote RF $E_{||}$-field on local antenna-plasma interactions by DC-biasing of the field lines due to the rectified sheaths on the opposite antenna side should be considered. This effect was observed in many experiments when a DC footprint of an active antenna was measured by a reciprocating probe several meters away from the antenna along the magnetic field lines [15, 16]. For the 3-strap antenna the influence of one antenna side on the other due to this DC effect is lower than that for the 2-strap antenna due to fact that on both antenna sides the RF $E_{||}$-field can be minimized simultaneously by the RF image current cancellation discussed next.

1.2 RF image current cancellation and $E_{||}$-field

Figure 2 shows the principle of minimization of the RF sheaths at the limiters, and the W sputtering consequently, by cancellation of RF image currents at the antenna limiters of the 3-strap antenna. Cases for a ratio of the power from the central strap to the power from the outer straps of P_{cen}/P_{out}=0.1, P_{cen}/P_{out}=2, P_{cen}/P_{out}=10 are shown from the left to the right accordingly. At $P_{cen}/P_{out}\approx$2, the RF image currents of these straps on the side limiters approximately cancel each other. The cancellation is achieved at both left and right sides of the antenna simultaneously, as opposed to the 2-strap antenna where only on one antenna side the cancellation is possible and was experimentally observed in [10].

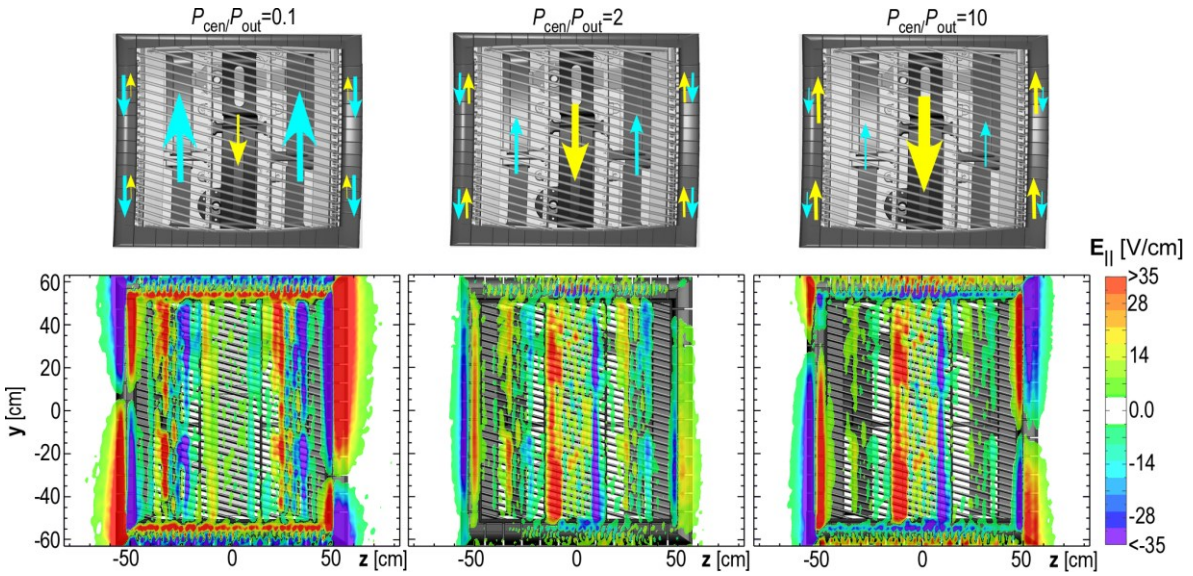

Figure 2. Upper row: RF image current cancellation close to power ratio of 2:1 (middle) in dipole phasing, compared to power ratio of 1:10 (left) and 10:1(right). The 3-strap antenna is shown using CAD view with every second FS rod removed. Lower row: corresponding TOPICA calculations of Re ($E_{||}$) at 36.5 MHz, 0.5MW power, in a plane in front of a flat model of the antenna.

The effect of the image current cancellation on $E_{||}$ is shown in the lower part of Fig. 2 by the calculations of *Re* ($E_{||}$) (dominant part of the fields) in front of the antenna by the linear electromagnetic TOPICA code [17] for a flat AUG 3-strap antenna model. The coordinate system for Fig.2 is the same as in Fig.1, except that z corresponds to pure toroidal and y corresponds to pure poloidal directions. The antenna aperture, a boundary between the vacuum region of the antenna and the plasma region described by the FELICE code [18] embedded in TOPICA, was set radially closest possible to the antenna limiters, in order to minimize filtering of small-scale RF fields. The plasma conditions and antenna settings correspond to AUG discharges #32445 and #32002 discussed below.

As implied in section 1.1, we consider the values of $E_{||}$ at the side limiters to be dominant. The $E_{||}$ maps in Fig. 2 suggest that this is a reasonable assumption in all the cases shown: the field at the limiters is typically higher than the field close to the outer straps (closest to the limiters) and the field close to the central strap is too distant to have a strong effect on RF sheath driving voltage on the side limiters, considering the parallel decay discussed above.

It is important to note that the reduction of $E_{||}$ by cancellation of the RF image currents on the antenna side limiters is location dependent. Whereas on the upper and on the lower sections of the limiters values of $E_{||}$ close to zero are achieved in dipole phasing and P_{cen}/P_{out}=2, the regions around y=0 are characterized by a higher $E_{||}$-field. Unique diagnostics which measures local measurements of the RF current at the limiters in AUG allows to check if a similar behaviour is observed in the experiments and if these RF currents indeed correlate with W sputtering.

2. Experimental results and discussion

2.1 Experimental setup

ASDEX Upgrade experimental setup with toroidal arrangement of ICRF antennas starting from the 2015 experimental campaign is presented in Fig. 3a. Four ICRF antennas, named *a1* to *a4*, are used with standard hydrogen-minority scheme in deuterium (D) or in helium (He). For this paper data from discharges with the toroidal magnetic field of B_t=2.5 T and the working frequency of 36.5 MHz is used. Two 2-strap antennas *a1* and *a3* constitute one antenna pair which is powered by the 3dB hybrid scheme [19]. Antennas *a2* and *a4* have 3 straps which are powered using two 3dB splitters as shown in Fig. 3b.

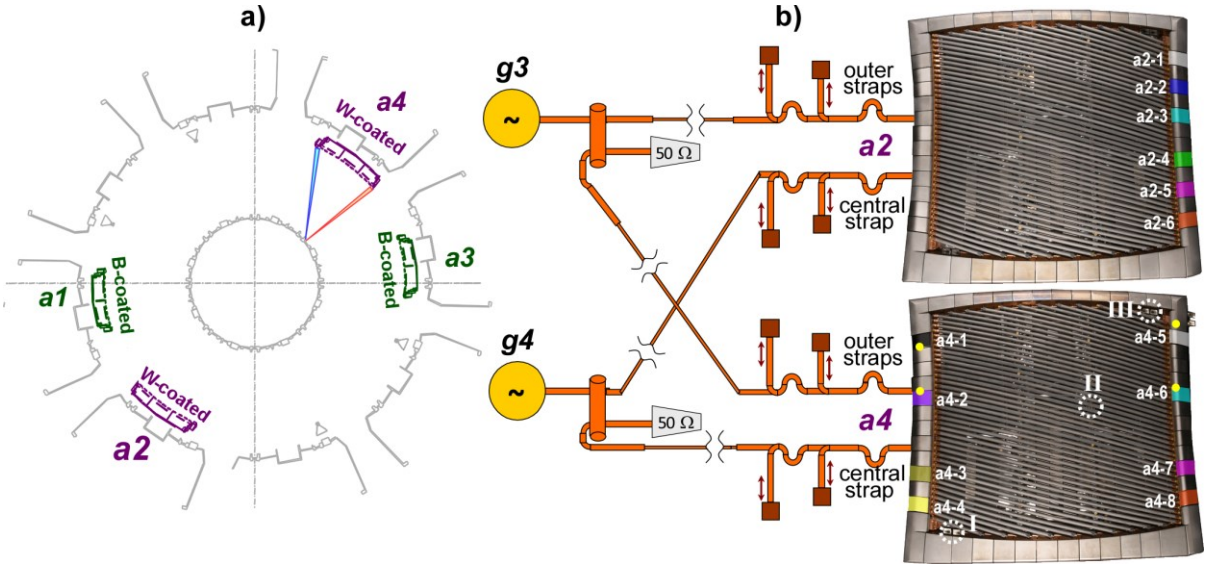

Figure 3. a) Toroidal view of ICRF antennas and spectroscopy views at a4 ASDEX Upgrade. b) 3-strap antenna connections; local spectroscopy (yellow circles) and the RF current measurements are shown on the antenna limiters; reflectometry locations I-III are indicated.

Both *a2* and *a4* are equipped with local RF image current measurements arranged as shown in Fig.3b, six on the right limiter of *a2* enumerated as *a2-1*…*a2-6* and four on each side of *a4*, enumerated *a4-1* to *a4-8*. At a fixed limiter geometry and loading conditions (plasma profiles), local amplitudes of electric field and of $E_{||}$ can be assumed directly proportional to the RF current measurements. Antenna *a4* has spectroscopic spots of observation in locations *a4-1*, *a4-2*, *a4-5*, *a4-6* which measure intensities of W I, 400.9 nm at and D I, 410 nm line spectral lines. The intensities are converted into W influx and effective W sputtering yield. For three locations in front of *a4*, indicated as *I*, *II*, *III* in Fig.3b, reflectometry measurements are installed [20] which resolve electron density profiles with the time resolution of 100 μs.

2.2 Antenna power balance in dipole phasing

Response of the RF current measurements at the limiters to a scan of the power balance between the central and the outer straps in dipole phasing for D H-mode discharge #32445, P_{aux}=5 MW and an addition of constant P_{ICRF}=1 MW from both *a2* and *a4* during scans is shown in Fig.4a. This discharge configuration allows for the RF power to be a relatively small perturbation. Thus the influence of the non-linearities connected to the changes of the core plasma during scans of antenna feeding parameters is small. At the same time ELMs were mitigated using the saddle coils [21] to provide calm conditions in the SOL. RF voltage equivalent for a 50 Ohm load in vacuum estimated from the RF current measurements is plotted as a function of P_{cen}/P_{out} for the six locations on the *a2* limiters. Every point corresponds to a time-average over 5 ms. Experimental data in Fig. 4a is compared to Fig. 4b with TOPICA calculations of the local $E_{||}$-field averaged spatially over the corresponding locations of the limiters. The absolute values of RF amplitudes in the experiment and in the calculations are not equivalent, because only vacuum calibration can be done for the RF measurements and that does not take into account influence of plasma on local RF circuit. Nevertheless, the relative behaviour can be compared. The measurements are well described by the local field magnitudes from the calculations, at least qualitatively. The tendency of the RF amplitude in the lower and the upper corners of the antenna (*a2-1*,*a2-2*,*a2-5*) to have a well-distinguished minimum is seen both in the measurements and in the calculations, as well as the tendency to have a more flat reaction to the power balance closer to the antenna middle (*a2-3*,*a2-3*,*a2-4*). Thus the local RF measurements at the limiters are represented well by the locally excited RF field calculated by TOPICA without taking into account the slow wave

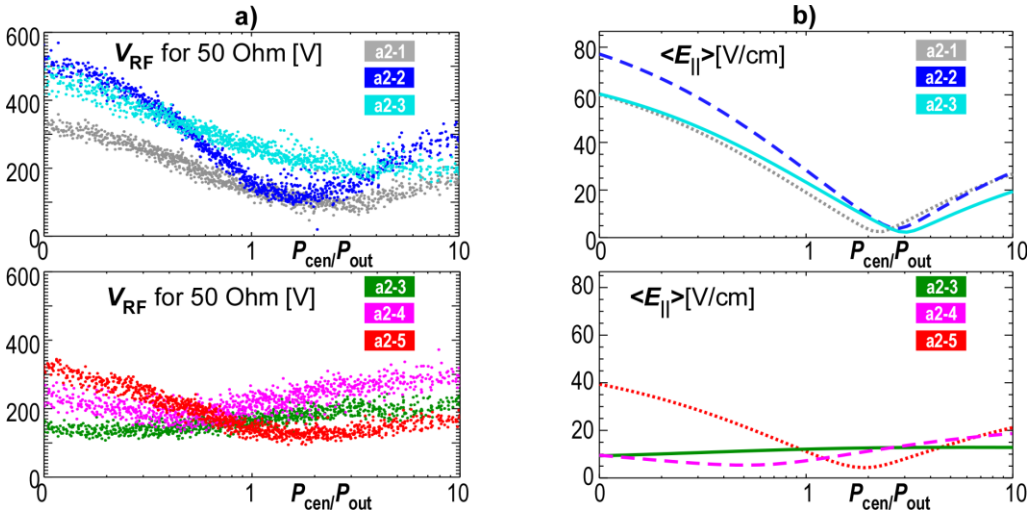

Figure 4. Dependency of RF amplitudes on a2 antenna limiters as a function of fraction of RF power from central strap: a) measured (5ms averages); b) calculated by TOPICA for flat antenna model.

propagation. However we note that the measurements are less responsive to the power balance scan than suggested by the calculations. The possible reason for this is discussed in section 2.4.

2.3 Phase-resolved amplitude balance and the W sputtering

A more sophisticated analysis than that in Fig. 4 can be done using both the scan of power balance P_{cen}/P_{out} and a scan of phase deviation from dipole $\Delta\Phi$. Figure 5 illustrates such two-dimensional dependency of the RF amplitude on the limiters V_{RF} of *a4* when both parameters were scanned simultaneously in discharge #32002 which has the same conditions as #32445. Plots in Fig. 5a correspond to the left *a4* limiter with locations from *a4-1* to *a4-4* and plots in Fig. 5b correspond to the right *a4* limiter with locations from *a4-5* to *a4-8*. We note that RF measurements on the limiters of the two 3-strap antennas *a2* and *a4* during the scans of the feeding parameters are not exactly the same. Antenna *a2* shows usually a more sensitive response, although main features of the dependencies remain similar. The reasons for this are likely related to small differences in alignment of the internal antenna geometry and to a diversity of the surroundings in the AUG vacuum vessel.

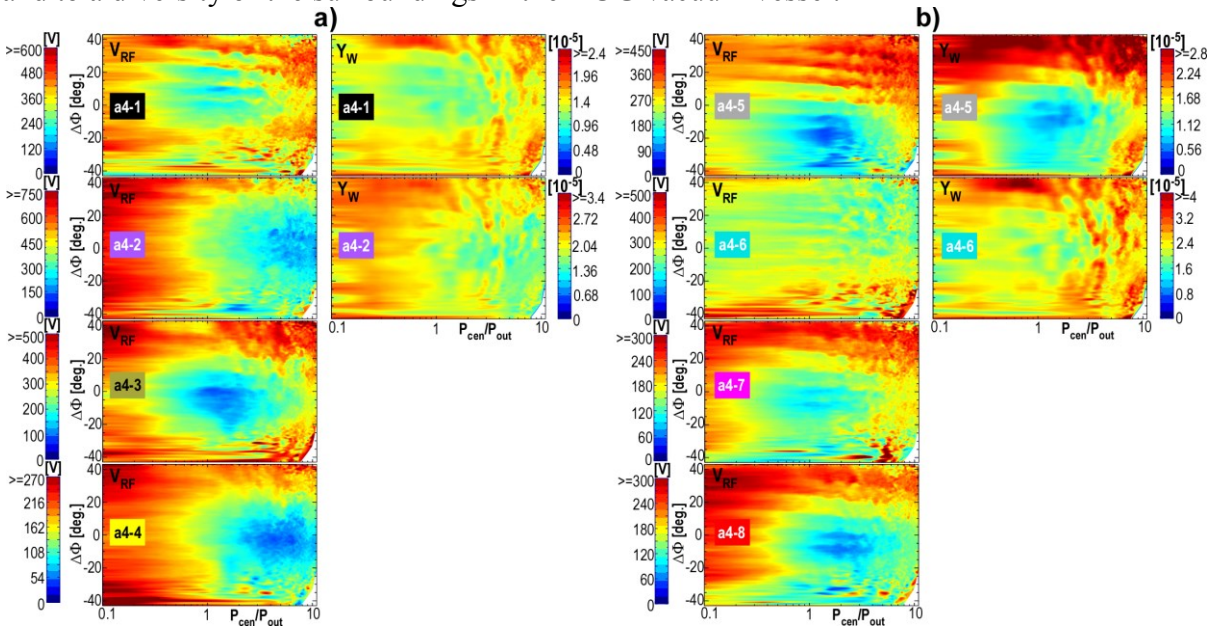

Figure 5. RF voltage (equivalent to 50 Ohm in vacuum) measured at the limiters of a4 and correlation to the W effective sputtering yield in the locations close to the RF measurements; a) left limiter of a4, locations a4-1 to a4-4; b) right limiters of a4 with locations a4-5 to a4-8.

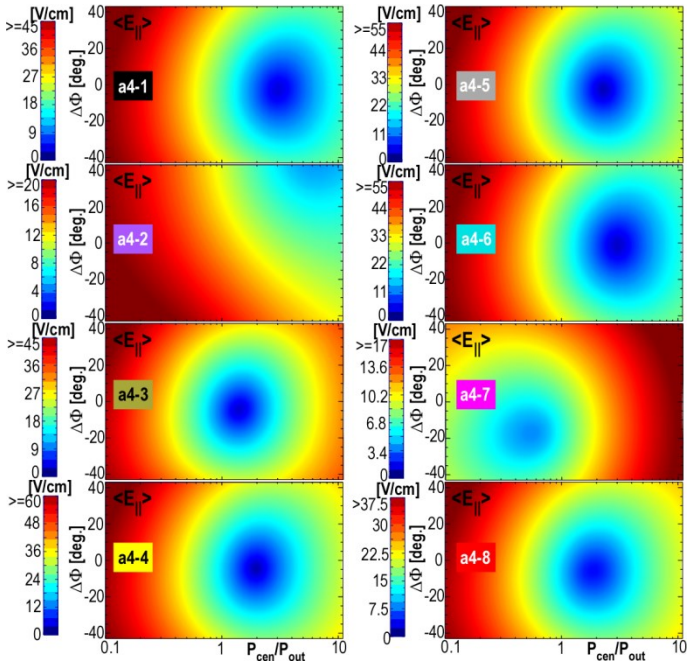

Figure 6. TOPICA flat-model calculations of spatially-averaged $E_{||}$ as a function of P_{cen}/P_{out} and $\Delta\Phi$ in the eight locations of a4 side limiters which correspond to the locations of RF measurements in Fig.5a (left column) and Fig. 5b (right column).

In addition to V_{RF}, Fig. 5 presents measurements of the effective W sputtering yield Y_W in locations *a4-1*, *a4-2*, *a4-5*, *a4-6* to the right of Fig. 5a and of Fig. 5b. Although the phase resolution of the data is limited, the minima of V_{RF} are visible which also approximately translate into regions with reduced Y_W. There is a good correlation between V_{RF} and Y_W, although these two quantities are connected through highly non-linear mechanisms which involve the RF sheath rectification and the W sputtering by the light impurity ions of carbon, boron, oxygen and nitrogen [2] with a certain distribution of concentrations and charge states. This provides a strong indication that, in order to reduce the W sputtering, one needs to reduce local values of the RF image currents and thus the sheath-driving RF voltages. However, the DC effect of plasma biasing on the field lines connected to remote RF current-carrying antenna components on W sputtering can also play a role. This effect could explain a slightly weaker reaction of Y_W to V_{RF} in locations *a4-1*, *a4-2*, *a4-4* which connect along magnetic field lines to the limiter at the other side and a stronger reaction in *a4-3* without a connection to the other side limiter.

The RF quantities from Fig. 5 can be compared to those of the TOPICA calculations discussed in section 2.2 for the dependence on the antenna power balance. The TOPICA results, now as functions of both P_{cen}/P_{out} and $\Delta\Phi$, are presented in Fig.6 for the same locations as in the experiments. The experimental measurements (Fig. 5) and the numerical results (Fig. 6) agree well on the existence of minima of the RF quantities and on the shifts of these minima with P_{cen}/P_{out}. The exact values of P_{cen}/P_{out} and $\Delta\Phi$ for the minima show a less good agreement in some locations, especially in locations *a4-2* and *a4-6* where the qualitative behaviour of the dependencies experiences a change.

Similarly to the data from Fig.4, the sensitivity of the RF response in the experiment is lower than that in the calculations. We hypothesize that, apart from the limited phase resolution of the data and deviations of the real geometry from the modelling geometry of the antenna, one of the main reasons are the strong temporal and spatial perturbations of the density profile in front of the antennas are present during the discharge.

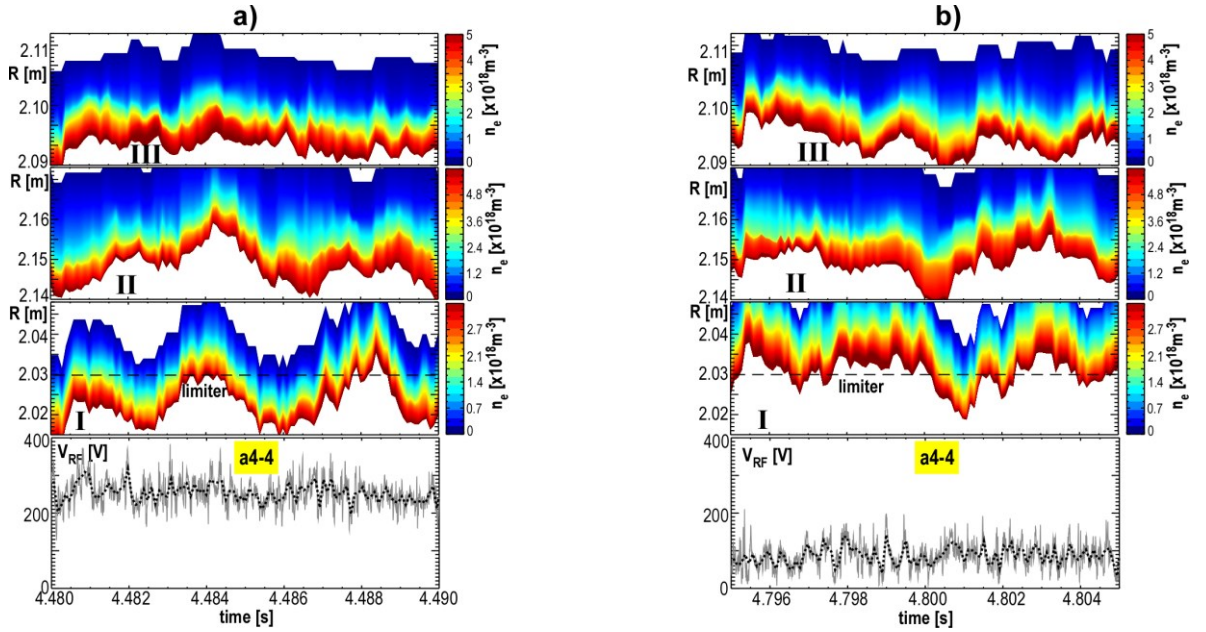

Figure 7. Electron density in front of a4 in #33336 in three locations from Fig.3b and RF amplitude in location a4-4 with signal averaged over 100μs shown by the black dotted curve. a) $P_{cen}/P_{out} \approx 0.1$; b) $P_{cen}/P_{out} \approx 2.5$.

2.4 Decorrelation of the RF image currents by density fluctuations

The previous analysis used time-averaged values from the experiment. However the time-resolved signals show significant fluctuations, as is illustrated in the example of the RF amplitude in location *a4-4* in Fig. 7. The imbalanced dipole case with $P_{cen}/P_{out}\approx0.1$ is plotted in Fig.7a and the balanced dipole case with $P_{cen}/P_{out}\approx2.5$ is plotted in Fig.7b together with the density profiles measured by the reflectometry at the three locations (*I*, *II*, *III*) in front of *a4* (see Fig.3b) in discharge #33336 with the same scenario as #32445 and #32002. For the reflectometry location *I*, the radial position of the antenna limiter for *a4-4* is shown by the dashed line. Although large ELMs are mitigated and only small intermittent events appear, the measured evolution of the density profile shows a high degree of spatial asymmetries.

Figure 7 shows that the RF amplitude at *a4-4* which is close to location *I,* does not clearly correlate with the density variation in *I*, despite the large variations. This seems to confirm that rather the asymmetric density distribution across the antenna influences the RF image current balance both globally and locally. Fluctuations of the toroidal and poloidal density distributions can decorrelate the contributions of the central and the outer straps and transiently make one of the contributions stronger.

Density distribution and asymmetries are also affected by the convective cells due to the DC biasing of the field lines induced by RF sheaths (see e.g. [22] and references therein). Indication of this phenomenon is observed in location *I* in the imbalanced case. Close to the radius of the antenna limiter, density in Fig.7a ($P_{cen}/P_{out}\approx0.1$) is on average lower compared to the balanced case in Fig.7b ($P_{cen}/P_{out}\approx2.5$). This complicates the situation even further and can enhance the density asymmetries.

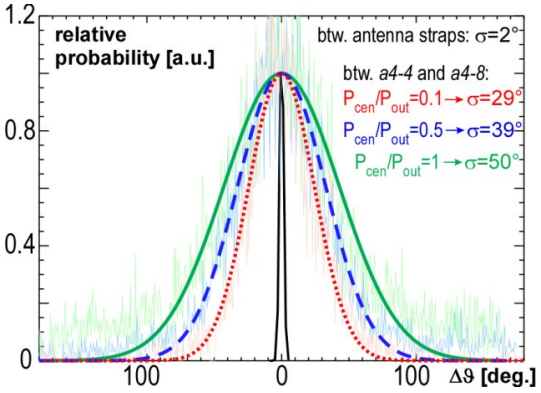

Figure 8. Histogram of deviation of the phase between the a4 straps (black) and between antenna limiters a4-4 and a4-8 for various P_{cen}/P_{out}.

Another evidence of the decorrelation of the RF image current contributions is presented in Fig. 8, using the information on deviation $\Delta\vartheta$ of the RF phase measured between the antenna limiters *a4-4* and *a4-8*. Despite the fact that the strap phasing is controlled within the small uncertainty of σ=2° (σ is the standard deviation in the Gaussian distribution), a large phase uncertainty of σ=29° is observed on the antenna limiters even when the contribution from the outer straps on the RF image current is dominant at $P_{cen}/P_{out}\approx0.1$. When the power ratio is increased towards the conditions of better RF local current cancellation, the intermittency of the plasma is accompanied by a more even competition between the strap contributions to the local RF current. This translates into a higher phase uncertainty with σ=39° for $P_{cen}/P_{out}\approx0.5$ and with σ=50° for $P_{cen}/P_{out}\approx1$. For the power ratio of $P_{cen}/P_{out}\approx2.5$ and higher, when the time-averaged local RF amplitude reaches a minimum, the phase uncertainty approaches 180°, because a small perturbation of the density profile can define whether the contribution from the outer straps or the 180°-phased contribution of the central strap is stronger. With this large phase uncertainty the net RF current is still relatively small. However zero cannot be reached on average, because the 3D density distribution needed for full RF current cancellation is very specific. This mechanism can explain why the modulation level of fluctuations of the RF amplitude in Fig.7b is larger than that in Fig.7a, as well as the fact that in sections 2.2 and 2.3 the TOPICA calculations for the homogenous plasma density profiles show the higher sensitivity to the variation of antenna feeding parameters than in the experiment.

2.5 Reduction of total W release

The local minima of the RF current and of the W sputtering yield discussed in sections 2.2 and 2.3 contribute to a minimum of the total W source, although not all of those are aligned to each other. Fig. 9 shows the ICRF-specific change of the W concentration Δc_W measured close to T_e=1.5 keV as a function of the strap power ratio P_{cen}/P_{out} in dipole phasing in #32445 discussed in section 2.2. The minimum of the increment of the W content is observed for P_{cen}/P_{out} between 1.0 and 3.0. This is consistent with the values of P_{cen}/P_{out} expected from the minima of the local quantities which were in their turn to a large extent consistent with the TOPICA calculations (Fig. 5). Therefore the local W source modulation is likely responsible for the minimum of the W content. This also means that the role of modifications of the $k_{||}$-spectrum during the scan of P_{cen}/P_{out} [23] is likely less important. However the $k_{||}$-spectrum defines the RF power absorption and coupling – its modifications could affect the antenna-plasma interactions and in general should not be neglected.

The W release of the 3-strap antenna at P_{cen}/P_{out}=0.1 is higher than that for P_{cen}/P_{out}=10. This is in a qualitative agreement with Fig. 2 which shows overall higher $E_{||}$-field at the limiters for the former case than for the later. This can be explained by the cross-coupling between the antenna straps which is taken into account in TOPICA calculations. The configurations with high P_{cen}/P_{out} induce RF currents in the outer straps keeping the current distribution on the straps more favourable for the lower $E_{||}$-field at the limiters than in the configurations with low P_{cen}/P_{out}.

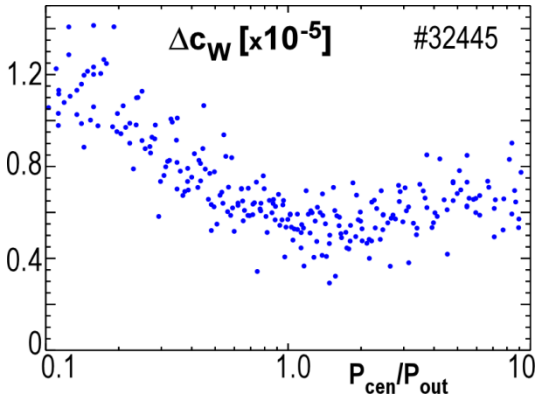

Figure 9. Influence of power balance in dipole on ICRF-specific W content in the core plasma (at T_e≈1.5keV). Every point is 20 ms average.

The basic comparison between the 3-strap and the 2-strap antennas based on the electromagnetic calculations was done in [3]. In order to estimate a reduction of the W production by the 3-strap antenna compared to the original 2-strap antenna, the rectified sheath potential $V_{DC\ sheath}$ can now be estimated, as physically the closest electrical quantity to the W sputtering yield. The estimate is made by using the asymptotic version of the SSWICH code [12] which calculates $V_{DC\ sheath}$ on the basis of the RF field maps in front of the antennas from the RAPLICASOL code [24]. Figure 10 presents the calculations of a poloidal-radial distribution of $V_{DC\ sheath}$ on the leading edge of the antenna side limiter using the radial distance from the leading edge Δx, both for the original 2-strap (left) and for the 3-strap (right) antenna with P_{cen}/P_{out}=2.0. The 3-strap antenna is characterized by about a factor of 2 to 3 reduced $V_{DC\ sheath}$ compared to the 2-strap antenna. This antenna improvement is roughly consistent with the experimental results which are presented in Fig. 11 where the antenna W release performance is compared relatively to the B-coated antennas in D-discharges. The figure shows the W content in the core plasma as well as the W influx Γ_W and the effective W sputtering yield Y_W averaged over the measurements on the upper half of the right limiter of *a4* for the 2-strap antenna (2014, Fig.11a) and the 3-strap antenna (since 2015, Fig.11b) configurations with details of the measurements locations described in [3] and in [25] correspondingly. A broad range of parameters is covered during the scans of the plasma triangularity δ_{upper} and the radial plasma position R_{out} (see details on the effect of δ_{upper} and R_{out} on ICRF-specific sputtering in [2,26]) for P_{aux}=5 MW and P_{ICRF}=1.5 MW, with the latter toggling between the antenna pairs. The relative differences with respect to the B-coated antennas in Fig.11a and in Fig11b help to estimate the improvement of the W-coated 3-strap antennas compared to the W-coated 2-strap antennas. In the whole range of the parameters, the use of the W-coated 3-strap antennas significantly reduced the W release. Around a factor of 2 or higher reduction of Γ_W and Y_W is observed, although these quantities are non-linear functions of $V_{DC\ sheath}$ and should be compared to the latter with care.

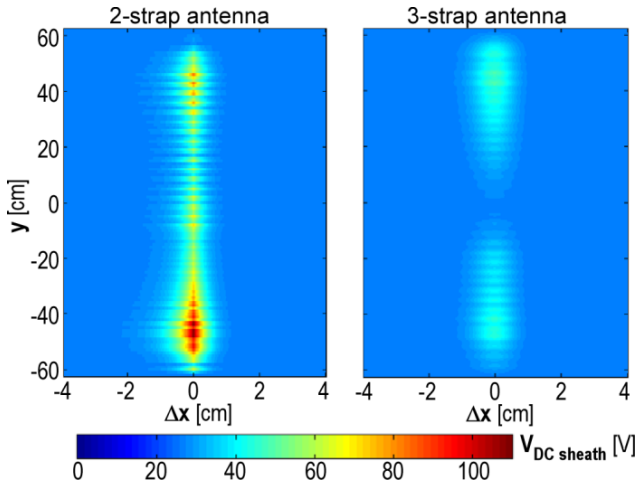

Figure 10. SSWICH calculations of $V_{DC\ sheath}$ with flat models of 2-strap (left) and 3-strap (right) antennas for 1 MW per antenna.

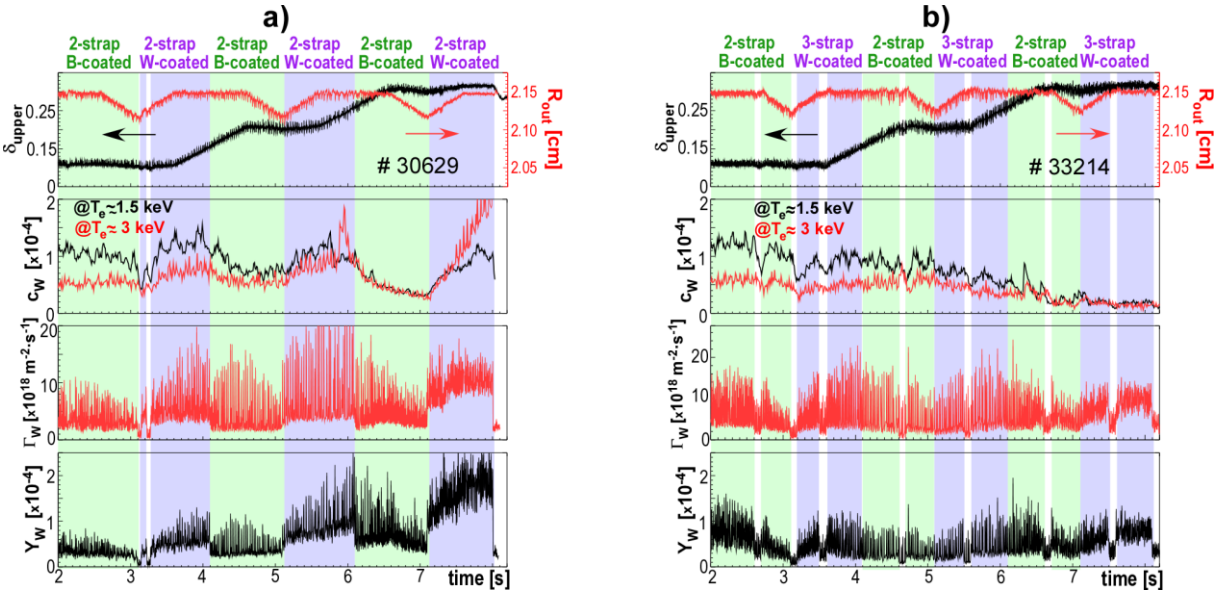

Figure 11. Comparison of the B-coated antennas with the W-coated antennas during scans of plasma triangularity and radial position in deuterium. Every antenna pair P_{ICRF}=1.5 MW in highlighted time windows on top of P_{aux}=6.3 MW. a) 2-strap antennas are W-coated (2014); b) 3-strap antennas are W-coated (since 2015, see Fig.3).

It is interesting to look at the He-discharges, because these strongly expose the ICRF-specific W sputtering and provide further information on the distribution of the W sources. In He, the W sputtering is amplified by a typically lower plasma density in the SOL and by the fact that He can sputter W directly in the range of ion energies in the SOL associated with the AUG ICRF operation [16]. The comparison of the W release between the 2-strap B-coated and the 3-strap W coated antennas in He characterized by c_W at T_e≈1.5 keV and by the increment of the total radiated power ΔP_{radtot} is presented in Fig.12 for #32664 with P_{aux}=4.8 MW. The W release associated with the 3-strap antennas is lower and the energy content response of the plasma ΔW_{mhd} is higher. This stands in contrast to the D-operation for which the plasma energy response [23] and c_W (see [23] and above) are usually very similar for both types of the antennas. One of the possible interpretations of this is that the remote W source (i.e. the W source which is not at the antenna limiters), which is presumably higher for the 2-strap antennas, becomes more important in the He-discharges. The increase of density of neutrals in the divertor shown in Fig.11 when the 2-strap antennas are active would be consistent with a stronger plasma-wall interactions leading to an outgassing.

Finally, one has to note that the improvement by the 3-strap antennas comes with a price of about 20% higher maximum RF voltage in the antenna transmission lines compared to the 2-strap antenna, although the radiating area was increased by about 20%. Moreover, the distribution of the RF power between the RF generators is uneven, because of the imposed P_{cen}/P_{out}> 1.0. Addition of another RF generator to the circuit of the central straps, planned for implementation in ASDEX Upgrade, will provide the possibility to use all RF generators at full power.

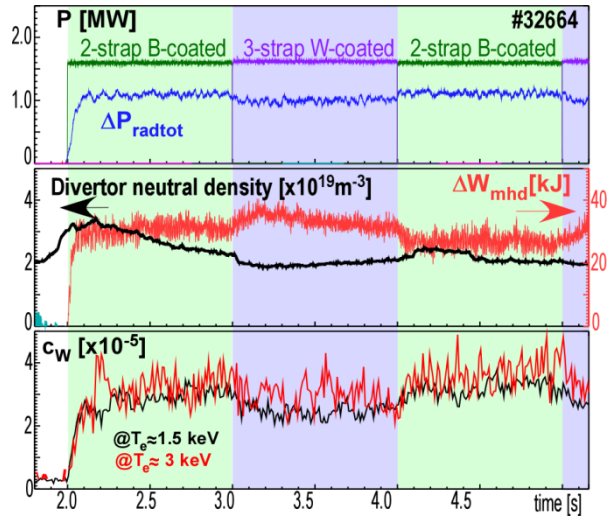

Figure 12. Comparison of the B-coated 2-strap antennas with the W-coated 3-strap antennas in He-discharge #32664.

Summary and Perspectives

Agreement between RF measurements at the antenna limiters in ASDEX Upgrade and TOPICA simulations points to the local E-field at the limiters as one of the main drivers of the RF sheaths. This is the case when the slow wave is evanescent and experiences a strong decay along the parallel distances smaller than the characteristic parallel dimensions of the antenna. Using the antenna power balance ratio and the strap phasing as variables for the 3-strap antenna, local minima of the RF current at the limiters and of the W sputtering yield can be achieved in various locations of the antenna limiters. These minima do not always align with each other at the same values of the variables. A design of an antenna which would have location independent minima in a broad range of loading conditions is challenging. Additional complication is the uncertainty of reaching these minima imposed by intermittent density profile fluctuations and asymmetries which are also non-linearly linked with the local ICRF-induced density convection. Nevertheless the 3-strap antenna with the W-coated limiters showed a significant reduction of the W release compared to the W-coated 2-strap antennas in a broad range of the plasma conditions. This reduction is approximately consistent with the non-linear estimates of the rectified sheath voltage in front of the antennas by the asymptotic SSWICH code which currently takes into account only the slow wave propagation in the SOL and in the future will implement the SOL fast wave propagation [27].

Thus, in order to reduce the plasma-wall interactions close to the antenna in the future ICRF antenna designs, the E-field needs to be reduced primarily on the radially protruding structures where the RF sheaths can form. This implies minimization of the RF currents on such structures. As a matter of fact, this can also mean a reduction of the antenna power launched per area as in the case of the 3-strap antenna.

As has been estimated in the past [23], the local W source from the antenna limiters, mostly affected by the antenna RF near-fields, was responsible for about 2/3 of the W content in the plasma core. Once this has been eliminated by the boron coatings on the limiters and dramatically decreased by the 3-strap antennas, the remote W source and the far-field effects are becoming increasingly more important. Thus the area of the future studies should include the minimization of the remote W sources by affecting the global RF field structure [28] in the experiment using such actuators as, e.g. phasing between the antenna pairs.

Acknowledgements

This work has been carried out within the framework of the EUROfusion Consortium and has received funding from the EURATOM research and training programme 2014-2018 under grant agreement No 633053. The views and opinions expressed herein do not necessarily reflect those of the European Commission.

References

[1] Neu R. et al 2007 *Plasma Phys. Control. Fusion* **49** B59–B70
[2] Bobkov V. et al 2010 Nucl. Fusion **50** 035004
[3] Bobkov V. et al 2013 *Nucl. Fusion* **53** 093018
[4] Perkins F. 1989 *Nucl. Fusion* **29** (4) 583
[5] D'ippolito D.A. et al 1998 *Nucl. Fusion* **38** 1543
[6] Mendes A. et al 2010 *Nucl. Fusion* **50** 025021
[7] Garrett M.L. et al. 2012 Fusion Eng. Des **87** 1570-5
[8] Colas L. 2013 J. *Nucl. Mater.* 438 S330–3
[9] Wukitch S. et al 2013 *Phys. Plasmas* **20** 056117
[10] Bobkov V. et al 2015 *AIP Conf. Proc.* **1689** 030004
[11] Bobkov V. et al 2009 *AIP Conf. Proc.* **1187** *125*
[12] Colas L. et al 2012 *Phys. Plasmas* **19** 092505
[13] Jacquot J. et al 2014 *Physics of Plasmas* **21** 061509
[14] Colas L. et al 2016 *submitted to Plasma Phys. Control. Fusion*
[15] Kubič M. et al 2013 *J. Nucl. Mater.* **438** S509-12
[16] Colas L. et al 2014 AIP Conf. Proc. **1580** 259-62
[17] Lancellotti V. et al 2006 *Nucl. Fusion* **46** S476
[18] Brambilla V. 1993 *Plasma Phys. Contr. Fusion* **35** 41
[19] Goulding R.H. et al. 1996 *AIP Conf. Proc.* **355** 397-400
[20] Aguiam D. et al 2016 *submitted to Rev. Scient. Instr.*
[21] Suttrop W. et al 2011 *Phys. Rev. Lett*. **106** 225004
[22] Zhang W. et al. 2016 *submitted to Plasma Phys. Control. Fusion*
[23] Bobkov V. et al 2016 *accepted for publication in Nucl. Fusion*
[24] Jacquot J. et al 2015 *AIP Conf. Proc.* **1689** 050009
[25] Bobkov V. et al 2016 *submitted to Nucl. Mater. Energy*
[26] Bobkov V. et al 2007 *J. Nucl. Mater.* **363-365** 122-6
[27] Lu L. et al. 2016 *43rd EPS Conference on Plasma Physics, Leuven, Belgium* P2.068
[28] Ochoukov R. et al 2016 *submitted to Rev. Scient. Instr.*